35-YEAR CYCLE IN SOLAR ACTIVITY IN 1000-1900

©2025 N. G. Ptitsyna*, I. M. Demina

St. Petersburg Branch of the Pushkov Institute of Terrestrial Magnetism, Ionosphere and Radio Wave Propagation of the Russian Academy of Sciences (SPbF IZMIRAN), St. Petersburg, Russia

**e-mail: nataliaptitsyna@yahoo.com*

Received August 08, 2024

Revised September 17, 2024

Accepted September 26, 2024

We performed a Fourier and wavelet analysis of solar activity in the range between the period of the Hoyle magnetic cycle (~22 years) and the Gleisberg cycle (50-120 years) in 1000-1900. Two reconstructions of the number of sunspots from indirect data were used based on: a) the number of low-latitude auroras and b) the concentration of 14C in tree rings. Our analysis showed that in the spectra of both reconstructions, there is a pronounced stable variation with a period of ~30-40 years, which is present even during grand minimums/maxima. The source of this variation is the frequency modulation by the Suess cycle with a period of ~200 years, resulting in a three-frequency structure with carrier oscillation with a period of ~35 years and sideband periods of ~30 and ~40 years. Some difference in the obtained spectra of the two reconstructions may be due to the different contribution of closed and open magnetic fields in the restoration of solar activity from different indirect data.

DOI: 10.31857/S00167940250211e1

1. INTRODUCTION

Dark areas on the solar disk – sunspots – are the most spectacular and easily observed aspect of solar activity (SA). Systematic registration of spots began in 1610 when the telescope was invented. The numerical expression of the number and structure of spots in a certain time interval can serve as an indirect measure of SA. The most commonly used numerical index of SA is the Wolf number *W* or its corrected version *SN*. *W* is a combination of the number of spot groups and the number of individual spots, taking into account the correction associated with bringing observations of different observers to a unified system.

Number of sunspots *SN* from telescopic observations is known more or less reliably only for the last 400 years. Longer series of *SN* can be obtained using indirect data recorded in one way or another on Earth in historical epochs. These include, for example, information about the appearance of auroras, records of which in historical documents date back to the 5th century BCE [Schove, 1962; Keimatsu, 1968; Eddy, 1980; Silverman, 1992; Siscoe, 1980; Nagovitsyn, 2001; Feynman and Ruzmaikin, 2014]. In addition, data on cosmogenic isotopes preserved in Earth's natural archives are widely used, such as the concentration of radiocarbon in tree rings or the content of nitrates in polar ice [Muscheler et al., 2006; Usoskin et al., 2007; Travers et al., 2012; Nagovitsyn, 2014; Usoskin, 2017; Brehm et al., 2021; Kudsk et al., 2022].

SA is subject to quasi-periodic oscillations, the most famous and stable of which is the 11-year Schwabe cycle. In addition, the 22-year Hale cycle, the ~100-year Gleissberg cycle, and the ~200-year Suess cycle have been widely studied. The range of periods between the Hale cycle and the Gleissberg cycle is less researched. Interest in this range of SA variations is connected with the known 35-year Brückner climate cycle, established back in the 19th century. Since that time, repeated attempts have been made to associate it with a possible similar cycle in the number of sunspots *SN* . Brückner himself Brückner, 1890] could not detect a 35-year variation in Wolf numbers. Later studies have also shown that cycles with a duration of ~30-40 years do not manifest themselves in sunspot formation indices [Vitinsky et al., 1986]. In works of recent decades, variations with periods of 31.1, 38.6, and 47 years have been found in solar and geomagnetic data [Kane, 1999; Echer et al., 2004; Singh and Badruddin, 2014]. The authors of works [Raspopov et al., 2000; Echer et al., 2004] believe that the 31-year period in the spectra of *SN* is possibly a solar source of the 35-year Brückner cycle. The results of the work [Kane, 1999] indicate that the spectral characteristics of SA for earlier time intervals (before 1914) and later ones differ significantly. In particular, the author of the work [Kane, 1999] in the spectra of *W* for 1914-1996 identified the most significant peaks corresponding to periods of 5.3, 8.3, 10.5, 12.2, and 47 years. For earlier time intervals (1748-1827, 1828-1913), more or less significant peaks in the range of periods *T* ~30-40 years were not found.

Recently, some indications of the existence of a 40-year variation in certain characteristics of SA have been obtained. The presence of a cycle with a 36-year period was found when studying experimental data series on the frequency of magnetic storms [Veretenenko et al., 2020] using several short samples from the 19th and 20th centuries. Analysis of spectroheliograms from Mt. Wilson Observatory in the 20th century (1910-1976) showed that a 40-year variation was observed in solar rotation during this time [Bertello et al., 2020]. However, the authors [Bertello et al., 2020]

raise the question about the reality of such quasi-periodicity due to limitations of the method they used.

This work is a continuation of our research [Ptitsyna and Demina, 2024], in which the presence of a 30-40-year variation during certain time intervals was discovered in the series of *SN* reconstructed from auroras over 700 years. The purpose of this work is to study in more detail the variability of SA on a 900-year time scale in the period range of 25-50 years, which lies between the periods of the Hale and Gleissberg cycles. In addition, our task was also to search for a possible cause that could determine the presence of a 30-40-year cycle and variations in its amplitude and/or frequency. An important feature of our research is the use of two reconstructions of the sunspot number *SN* , obtained by fundamentally different methods: reconstructed based on data on historical auroras in 1000-1700 [Ptitsyna and Demina, 2020] and data on the production of the cosmogenic isotope ^{14}C in annual tree rings in 1000-1900 [Usoskin et al., 2021].

2. DATA AND METHODS

In this work, we analyze two reconstructed SA series SN_1 and SN_2, obtained from two fundamentally different sources of indirect information.

Series SN_1 covers a period of 700 years from 1000 to 1700 [Ptitsyna and Demina, 2020]. This reconstruction is based on observations of auroras in Europe, as well as in the European and Asian parts of Russia at middle and low latitudes (geomagnetic latitude $\phi<56°$). When synthesizing the series SN_1 the contribution of the Earth's main magnetic field was taken into account, and a normalizing conservative "civilizational" correction was applied, based on population growth and the number of Universities in Europe. The details of the reconstruction are described in detail in [Ptitsyna and Demina, 2020]. The number of auroras can serve as a measure of the numerical characteristics of SA and its variations, as the pattern of auroras reflects the pattern of SA. The features of this relationship depend on latitude [Siscoe, 1980; Liritiz and Petropoulos, 1987; Vasquez et al., 2014; Ptitsyna et al., 2017]. For auroral events recorded at middle and low latitudes, there is a direct correlation between the number of auroras and *W* .

Series SN_2 was reconstructed based on data on the production of the cosmogenic isotope ^{14}C in tree rings in England and Switzerland (geomagnetic latitude $\phi \approx 50°-62°$) [Usoskin et al., 2021]. This series covers the interval from 971 to 1899. Cosmogenic radionuclides are produced in the Earth's atmosphere by high-energy particles of galactic cosmic rays. Their atmospheric concentration depends on the particle flux and the level of SA. When reconstructing SA, the solar modulation parameter Φ is used, which is determined by the heliospheric/solar magnetic field shielding galactic cosmic rays. The concentration level of radionuclides is also influenced by the

Earth's magnetic field, the changes of which are also taken into account in the work [Usoskin et al., 2021]. The influence of climatic conditions can introduce a large uncertainty in the assessment of the transport of cosmic nuclides from the atmosphere to natural archives where they are stored.

Fig. 1.

Both series used in the study are shown in Fig. 1. The reconstructed series SN_1 (Fig.1 *a*) is presented in accordance with the work of [Ptitsyna and Demina 2020]. As the series SN_2, reconstructed from ^{14}C (Fig.1 *b*), we used annual values without smoothing in accordance with the work of [Usoskin et al., 2021], this series is available on the website (https://cdsarc.cds.unistra.fr/ftp/J/A+A/649/A141/osn.dat). Vertical lines mark the grand minima of Oort, Wolf, Spörer, and Maunder.

In Fig. 1, the difference in amplitudes between SN_1 and SN_2 is noticeable. The smaller amplitude of the series SN_1 (proportional to the number of auroras) occurs because its reconstruction used not all auroral events that occurred on Earth, but only the largest historical auroras visible at middle and low latitudes. Despite the systematic difference in amplitudes, the general nature of SA changes over time is clearly visible. In particular, for both series, global decreases and increases in amplitude (grand minima and prolonged maxima) are well aligned in time. To emphasize the similarity of these series, we smoothed them with a 40-year moving window and normalized to the maximum value. The result is shown in Fig. 1 *c* , with a solid line representing the reconstruction from auroras, and a dashed line representing the reconstruction from ^{14}C. The sample size was chosen so that it did not exceed the time interval of all grand minima. The general nature of the change in the time series under consideration is beyond doubt.

For the analysis of spectra SN_1 and SN_2 Fourier analysis and wavelet transform were used. The first has been known for a long time and is widely used in practice, as it allows to identify the main dominant periods, averaged over the considered time period. In recent decades, wavelet transform has been widely used for signal analysis [Daubechies, 1992]. The main difference between wavelet transform and Fourier analysis is that it allows to localize a signal of a given shape and obtain information about the spectral structure of the signal at individual moments of time and, as a consequence, about the change in time of the magnitude of periods present in the signal and their amplitude. In essence, the wavelet transform is a convolution of a given signal with the investigated time series, which provides the temporal localization of individual spectral components. The given signal is called the generating function. This function is scaled to different time intervals, and this gives the dependence of the spectrum on the scale of the generating function, which can be

converted into periods. Thus, the wavelet spectrum is a matrix that reflects the change in dominant periodicities over time. For details, see, for example, [Daubechies, 1992].

3. FOURIER ANALYSIS OF THE SERIES SN_1 AND SN_2

Primary estimates of the spectral composition of the analyzed time series were made based on the application of the Fourier transform to them. The result of the calculation is shown in Fig. 2 *a* . Since the original time series differ in intensity, and, as a consequence, the spectra differ quite significantly in amplitude, they are shown in different scales. The scale for each spectrum was chosen for clarity of presentation. The period axis is converted to a logarithmic scale, which allows for better resolution in the range of variations of interest to us.

Fig. 2.

Figure 2 *a* shows that the spectra of both series SN_1, SN_2 are dominated by an 11-year component and several peaks in the range of Gleissberg cycle periods T ~50–120 years, which stand out sharply in intensity. In addition, individual maxima can be observed in the period range of 25–50 years, which manifest in the SN_1 and SN_2 series to varying degrees. However, a clearly defined peak in this frequency range (T ~31.8 years) is present only for the SN_1 series. Further, all time series were passed through a bandpass filter with a bandwidth of 20–55 years. The spectra of the signals obtained as a result of filtering are shown in Figure 2 *b* . It was possible to noticeably redistribute the spectral power to the period range of ~30–40 years. Thus, for the SN_2 series, the intensity increased in the range from 25 to 50 years, with maxima around 35 years becoming clearly visible: in descending order of intensity 45.7, 26.1, 31.48 years (Figure 2 *b*). For the spectrum of reconstruction SN_1, the band of ~30-year periods was significantly enhanced. In addition to the dominant peak of 31.8 years, equivalent peaks of 43.75 and 21.88 years are visible.

In the spectrum of the time series of sunspot numbers SN , obtained from observational data for the last 300-400 years, among the many peaks besides the dominant 11-year one, peaks with periods T =22 and T >50 years were found [Petrovay, 2020]. In many works, short-term, inconsistent periodicities have been found, which differ for different data sets [Kane, 1999]. For some short intervals, peaks of 31.1, 38.6, and 47 years were found [Kane, 1999; Echer et al., 2004; Singh and Badruddin, 2014]. Thus, the results obtained in this paragraph for the reconstructed series do not contradict those obtained for the observational series, and their spectral characteristics allow us to hope for the identification of 30-40-year cyclicities at least at individual time intervals. For this, we will further conduct a wavelet analysis of the series SN_1 and SN_2 in the range of scales

corresponding to ~30-40-year periodicities, over a long time interval (1000-1900 years), which will reveal the variability of these periodicities over time.

4. CYCLICITY ANALYSIS SN_1 WITH A PERIOD OF 30–40 YEARS

4.1. Wavelet Analysis

In the Fourier transform result of the solar activity time series SN_1 reconstructed from aurora borealis, a 30–40-year component is clearly manifested. For a detailed analysis of the temporal spectrum variation in this range, we applied wavelet analysis. As the generating or basic function, the Morlet function [Grossman and Morlet, 1984] morl(x) = exp(- x^2/2)cos(5 x) was chosen, which represents a plane wave modulated by a Gaussian. The scales of this basic function are close in value to periods, which makes it easy to isolate the desired range during integration. Since the wavelet transform is a convolution of the signal and the generating function

$$\Psi(a,b) = \frac{1}{|a|^{1/2}} \int_{-\infty}^{\infty} f(t)\psi^*\left(\frac{t-b}{a}\right) dt, \qquad (1)$$

where f (t) is the analyzed signal, a is the wavelet scale, b is the shift, ψ is the generating function, by changing the scale, we are effectively changing the period, and the shift provides localization of this spectral component in time. As a result of calculating the convolution (1), we obtain a matrix of coefficients. For its visualization, a representation in the form of a contour map of the coefficient modulus is used. The result obtained for the series SN_1 is shown in Fig. 3. Symbols mark the maxima that we attributed to the 30- and 40-year components. Some of the observed maxima remained unmarked, as they correspond to periods < 27 years. It appears that these maxima may reflect the cumulative effect of contributions from changing periods of 30- and 22-year components. Due to the small difference in frequencies of these components, the band-pass filtering performed cannot completely separate the contributions of such close periods.

Fig. 3.

Figure 3 shows the stable presence of 30- and 40-year cycles, the period of which changes over time. It should be noted that in some time intervals (1000-1070 and 1200-1420), two branches with periods T_1~30 years and T_2~40 years are simultaneously present. The branches of this variation are also well traced during the grand minima of Oort (1020-1080), Wolf (1265-1345) and Spörer (1400-1540) and long maxima (~1080-1250, ~1350-1400, and ~1550-1625). Unfortunately, it is not possible to assess the presence of the 30-year cycle during the Maunder Minimum (1650-1710), as the edge effect is already making an impact here. From 1200, the

branches with periods T_1 and T_2 are in a sort of anti-correlation. We hypothesized that the presence of such a pattern may be due to the modulation effects of a longer-wave process.

4.2. Modulation

In frequency modulation, the period of the fundamental oscillation changes depending on the amplitude of the modulator. The main characteristics are the deviation or the maximum deviation of the frequency (period) of the fundamental oscillation from the average, and the modulation index K, which determines the degree of influence of the modulator on the main signal. The concept of frequency modulation and all its properties are developed for harmonic signals. The main difference between frequency modulation and amplitude modulation is that in amplitude modulation, the signal amplitude changes over time with the periodicity determined by the modulator, but not its period, while in frequency modulation, the opposite occurs - the period changes, but not the amplitude. Moreover, in the spectra of the resulting signal in both cases, additional combination harmonics appear. In the case of frequency modulation, their number and amplitude ratio depend on the index $K = \Delta\omega/\omega_m$, where $\Delta\omega$ – is the maximum deviation, or frequency deviation, and ω_m is the modulator frequency. The time series we are considering are not harmonic or a sum of harmonic signals. We assume the presence of quasi-periodic components in these series. And, judging by the change in individual spectral components in the wavelet spectra, the original signals are subject to both amplitude (intensity change) and frequency (period change) modulation. In general, in the case of non-harmonic signals, the influence of the modulator (also non-harmonic) is complex, but earlier in the work [Ptitsyna and Demina, 2023], we modeled the frequency modulation of the 11-year cycle, which resulted in a wavelet spectrum that exhibited all the features characteristic of the wavelet spectrum of the original signal. This allowed us to assume that to test the hypothesis about the role of frequency modulation in the formation of 30- and 40-year components and to obtain an estimate of the period of a possible modulator, it is possible to use the basic formulas describing frequency modulation. If A_0 and ω_0 are the amplitude and frequency of the original signal, and ω_m is the frequency of the modulator, then the resulting time dependence will be expressed by the formula

$$F(t) = \mathrm{A}_0 \sin(\omega_0 t + \Delta\omega \cos(\omega_m t + \varphi_m) + \varphi_0),$$

where φ_0 and φ_m are the corresponding phases. Then, setting the phases equal to zero, and $K = 1$ - in this case, the frequency deviation equals the modulator frequency - we get that the change in the frequency of the main oscillation can be written as

$$\omega(t) = \omega_0 + \omega_m \cos \omega_m t \ . \qquad (2)$$

From this, we obtain the relationship between the period of the main oscillation T_0, the period of the modulator T_m, and the periods observed in the spectrum T_1 and T_2. For the points of maximum frequency deviation (t =0), transitioning to periods, from (2) we get

$$\frac{1}{T_0}+\frac{1}{T_m}=\frac{1}{T_1} \quad \text{и} \quad \frac{1}{T_0}-\frac{1}{T_m}=\frac{1}{T_2} \quad . \tag{3}$$

Obviously, knowing T_1 and T_2 and adding the expressions in (3), we can obtain T_0. However, for this simple action, it is necessary to know T_1 and T_2 at the same moment in time and with the maximum difference between T_1 and T_2, primarily to reduce the influence of errors in determining each period on the final result. Note that to estimate T_0, knowledge of the exact value of the deviation is not required, since the frequency difference eliminates the dependence on ω_m. There are few such pairs of points, but they allow us to estimate T_0=35±1 years. To obtain an estimate of the modulator period using formula (3), exact knowledge of the deviation is already required. In our case, we need a pair of points that have the same time, and the deviation of periods from T_0 at these points is maximum. There are no pairs that exactly satisfy these conditions, and using points with properties close to the required ones causes a significant scatter in the result T_m=188±9 years. Note that the obtained results are of an estimated nature, since the time series under consideration do not represent harmonic signals.

Within the hypothesis of modulation of the main oscillation T_0 by a long-wave signal, a mirror branch can be constructed for each branch, taking as each branch the periods T_1 and T_2 obtained from the wavelet spectrum and using formulas (3), while considering the period of the main oscillation to be known and equal to the above estimate of 35 years. We will further call the constructed mirror branches the predicted periods. In essence, the periods of the side branches continuously change synchronously with the amplitude of the modulator, but for brevity, we will henceforth refer to them as the 30-year and 40-year branches.

Fig. 4.

In Fig. 4, black circles show the change in the period of the 30-year branch, and black diamonds show the same for the 40-year branch. Based on the period values of the 30-year branch, the predicted values of the 40-year branch periods were calculated, shown in Fig. 4 as unfilled diamonds. Conversely, based on the values of the 40-year branch, the predicted 30-year periods were calculated, shown in Fig. 4 as unfilled circles. It can be seen that some highlighted points differ significantly from the predicted ones. However, if we look at the position of these spectrum maxima in Fig. 3, we can notice that these points fall in areas of strong influence of shorter periods on the 30-year ones, i.e., the period values of 27-28 years most likely do not purely relate to the 30-year

branch. It can be assumed that the long-wave ~200-year component modulates not only the 35-year cycle in frequency and, as we previously obtained [Ptitsyna and Demina, 2022], the Gleissberg cycle, but the same effect can be expected for the 22-year component. For this component, the frequency/period deviation in this case would be 2-3 years. And if, by analogy with the 11-year component, we assume the influence of the Gleissberg cycle, then the deviation could be 7-8 years. In this case, the spectra of the lower branch of the 35-year and the upper branch of the 22-year would significantly overlap.

It should be noted that in Fig. 3, the side branches are clearly visible, while the main frequency T =~ 35 years is practically not identified as a separate branch. It must be kept in mind that the difference between the periods of the main oscillation and the side branches does not exceed 10 years, which, with a period scale step of 1.23 years, creates great difficulties in distinguishing all 3 branches of different amplitudes. However, in Fig. 4, it can be seen that the main frequency is nevertheless indirectly well manifested in the change of the side branches. The change in the nature of the variation of the 30- and 40-year branches from growth to decrease (branches converging and diverging) occurs precisely at period values of ~35 years. This additionally supports the hypothesis about the nature of the 30- and 40-year branches as a manifestation in the spectrum of frequency modulation by a long-wave process of the main oscillation with a period of ~35 years.

5. ANALYSIS OF CYCLICITY SN_2 WITH A PERIOD OF 30–40 YEARS

5.1. Wavelet analysis

The same processing stages were applied to the time series SN_2 as to the series SN_1. The resulting wavelet spectrum is shown in Fig. 5.

Fig. 5.

The periods identified reflect the general character of the series spectrum SN_2, shown above in Fig. 2. Additionally, Fig. 5 shows the same trends as for the wavelet spectrum of SN_1 (Fig. 3). In the spectrum of SN_2 there is a stable presence of a 30-40-year variation, consisting of two branches with periods $T \approx 30$ and $T \approx 40$ years throughout the entire time interval (1000-1900), including during grand minima, such as the Maunder Minimum (1610-1710), and prolonged maxima. However, this mainly applies to the branch with a 40-year period, as the 30-year cycle is less distinct against the background of period changes in the 22-year variation band. The growth of the latter's period to 26-27 years, as was also observed for the SN_1 series, makes the separation of the increasing 22-year and decreasing 30-year cycles practically impossible. If we compare the integral intensity of the spectrum in the bands of 22-27 years (I_1) and 28-33 years (I_2), then for the time interval 1080-1180, their ratio is I_2 / I_1 =1.19, and the 30-year branch can be identified, while for the time interval

1750-1850, this ratio is 0.77, and the 30-year branch is not distinguishable. It can also be noted that the 30- and 40-year branches, as in the spectrum of the SN_1 series, demonstrate a tendency toward anti-correlation. However, it is clearly visible that the 40-year component mostly lies above 45 years, while the 30-year component has the greatest intensity in the 27-30 year band, which may be a direct consequence of the influence of the 22-25-year and 50-60-year components, whose dominance remained in the spectrum of SN_2 even after filtering (Fig. 2). As a result of this influence, the periods of the 30- and 40-year components obtained from the spectrum may be underestimated and overestimated, respectively. At the same time, precisely because the 30- and 40-year components strongly "diverge," periods close to 35 years can be seen in the wavelet spectrum (marked with asterisks in Fig. 5). According to our hypothesis about frequency modulation, 35 years is exactly the period of the main oscillation, while 30 and 40 years represent the result of frequency modulation observed in the spectrum. Only 3 pairs of points belonging to different branches and suitable for estimating the modulator period were found. The modulator period estimated from them was 205±53 years. The error is quite significant, but it should be kept in mind that the obtained estimates are strongly influenced by both the 50-60-year and 20-25-year components.

5.2. Modulation

Let's display the changes in periods on a separate graph and calculate the predicted values of the 30- and 40-year branches assuming frequency modulation of the 35-year oscillation, as was done above for the SN_1 series. The result is shown in Fig. 6.

Fig. 6.

Comparison of the predicted period values with those obtained from the wavelet spectrum shows that the greatest difference is observed during periods of maximum influence of 50-60-year variations (1050-1150, around 1400 and 1700). For these time intervals, the period values in the spectrum are clearly overestimated.

Our assumption about the nature of the 30- and 40-year oscillations as a result of frequency modulation of the 35-year component by a long-wave process suggests that for the two time series under consideration SN_1 and SN_2, obtained based on different data, this modulator should have the same period and phase. Regarding the period, similar values were obtained, practically within the margin of error (T_m=188±9 years for the series SN_1 and 205±53 years for the series SN_2). As for the phase characteristic, for comparison, Fig. 7 separately shows the predicted values calculated for the series SN_1, here they are designated as ✲ for the 30-year branch and as ✳ for the 40-year branch.

Fig. 7.

The density of points for the 4 branches under consideration is not sufficient for their reliable comparison, but we can identify one time interval each for the 40-year and 30-year branches where the values of the predicted periods SN_1 and SN_2 form continuous segments. These time periods are highlighted by rectangles in Fig. 7. For the 40-year component, the correlation coefficient k between the predicted periods SN_1 and SN_2 was 0.7. To evaluate the possible shift, the cross-correlation function (CCF) was calculated. The result is shown in Fig. 8 *a* . Its maximum was shifted by 10 years, which actually lies within the range of variation of the 40-year component period. For the 30-year branch, due to gaps and individual sharp deviations, interpolation was performed using smoothing cubic splines. In the analyzed changes of the predicted 30-year periods, there was a linear trend that was removed for calculating correlation characteristics. As a result, the calculated correlation coefficient was k =0.4, and the CCF showed a broad maximum at zero with two additional peaks of almost equal value: 0 and −36 years (Fig. 8 *b*). The maximum symmetric to the latter is poorly expressed and can only be estimated as 40 years. These additional maxima are close in value to the period of the presumed main oscillation, which indicates the presence of such periodicity in both time series. In addition to the broad maximum at zero in the CCF of the 30-year branches, there are two more symmetric maxima, with one of them having the maximum correlation. These maxima correspond to a shift of ±235 years, which indicates the presence of such a long-wave periodicity in both time dependencies. This fact can be considered as further evidence supporting the hypothesis that the 30- and 40-year branches are manifestations of frequency modulation of the main 35-year oscillation by an approximately 200-year long-wave signal.

Fig. 8.

The presented results provide grounds for a hypothesis about the presence of a hierarchical structure of periodic components in SA, with longer-wave components influencing the generation of shorter-wave ones, which appears in the spectrum as a result of frequency modulation.

6. DISCUSSION OF RESULTS

Our analysis showed that during the second millennium, 30- and 40-year variations are consistently present in the spectra of SN_1 and SN_2, even during the medieval grand maximum and the grand minima of Oort, Wolf, Spörer, and Maunder. In general, the time evolution of the periods of 30- and 40-year variations can be related to frequency modulation by a longer-period process, namely the Suess cycle ($T \approx 200$ years) of the main oscillation with $T \approx 35$ years. As a result, a three-frequency structure of this variation is formed with periods of side branches varying in the ranges $T_1 \approx 28 \div 35$ and $T_2 \approx 35 \div 45$ years and the main period $T_0 \approx 35$ years. However, the main 35-year branch is very weakly visible against the background of the side branches for both series. Such

a pattern without the main frequency can be observed under certain ratios of parameters of the modulated and modulating signals, which is often used in radio engineering practice to reduce the energy share that falls on the carrier frequency of signals [Gonorovsky, 1977; Connor, 1982; Baskakov, 2016].

In this context, let's turn to the results of [Ptitsyna and Demina, 2022], which found that the Gleissberg cycle consists of three distinct branches with periods of 60, 88, and 140 years, with the formation of these branches occurring as a result of a modulator with a period $T \approx 200$ years, i.e., the Suess cycle. From the model calculations conducted by the authors of [Ptitsyna and Demina, 2022], it follows that for a frequency-modulated signal with sufficiently high modulation coefficient values, the main 88-year period may be significantly smaller in amplitude than the side components, and at certain points in time it may be practically indistinguishable in the spectrum against their background. This is how the authors of the study [Ptitsyna and Demina, 2022] explain the fact noted in many works [Clilverd et al., 2006; McCracken et al., 2013; Svalgaard, 2018] that the 88-year Gleissberg cycle is poorly traced in the modern era. By analogy with the results of [Ptitsyna and Demina, 2022; 2023], it can be assumed that due to the properties of frequency modulation, the main period of ~35 years appears clearly in the spectrum only at certain times throughout the interval of 1000-1900.

In the paper [Ptitsyna and Demina, 2023], it is shown that variations in the length of the solar cycle over the past 320 years can be described within a model representing an 11-year oscillation that undergoes frequency modulation by branches of the Gleissberg cycle (60 and 115 years) with a time-varying influence of the modulator. That is, in this case, the Gleissberg cycle acts as the modulator. Thus, we can conclude that in the system of SA variations, there appears to be a hierarchy of cycles interconnected by modulation effects. In the theory of oscillations and nonlinear dynamics, it is known that a hierarchical system of oscillators and modulators can synchronize at certain moments to create a stable rhythmic pattern, and sometimes transform into chaos [Landa, 1997]. The authors of [Feynman and Gabriel, 1990] adhere to the view that the solar dynamo, which generates SA variations, functions in a chaotic regime. The study [Usoskin et al., 2007] suggests that the solar dynamo functions in a quasi-periodic regime throughout the extent of SA reconstructions, except during grand minimum/maximum periods, where the quasi-periodic regime transitions to a state of chaos. In contrast to these conclusions, our results showing that on a millennial scale in *SN* series, even during grand minimum/maximum periods, stable 30- and 40-year variations are observed, whose periods undergo changes according to the laws of frequency modulation, indicate much greater regularity in SA variations and, thus, in the functioning of the solar dynamo. The

results of this article, taking into account the aforementioned conclusions of works [Ptitsyna and Demina, 2022; 2023], allow us to say that the solar dynamo mainly functions in a quasi-periodic regime. This conclusion is consistent with the opinion of the authors of the work [Peristykh and Damon, 2003], who believe that their finding of a stable 88-year cycle over a time interval of ~11000 years does not support the idea of quasi-chaotic behavior of solar processes on scales longer than 11 years.

Despite the fact that both series SN_1 and SN_2 exhibit similar stable variation with a visible predominance of two branches with periods $T_1 = \sim 30$ and $T_2 = \sim 40$ years, the branches themselves, constructed for the series SN_1 and SN_2, and predicted as a result of frequency modulation differ from each other. The correlation coefficients between the predicted changes in periods of SN_1 and SN_2 for the 40-year branch was $k = 0.7$, and for the 30-year branch $k = 0.4$. We believe that this difference in spectra is due to the difference in the methods of data reconstruction for SN_1 and SN_2. These reconstructions of *SN* are based on obtained ground data (number of auroras for SN_1 and concentration of ^{14}C in tree rings for S N_2), reflecting changes in geomagnetic and heliospheric activity, which, in turn, are related to changes in SA and, accordingly, to solar magnetic fields.

Traditionally, it is considered that geomagnetic disturbances have two different sources in interplanetary space and on the Sun [Simon and Legrand, 1989; Gonzalez et al., 1994; Tsurutani et al., 2006; Vasquez et al., 2014]: *a*) transient coronal mass ejections *CME* mainly from regions with closed field lines, such as active regions and spots; *CME* initiate magnetic storms with sudden commencement and *b*) recurrent high-speed streams *CIR* from coronal holes, which are characterized by open magnetic fields; *CIR* initiate magnetic storms with gradual onset [Borovsky and Denton , 2006; Obridko et al., 2013; Gopalswamy, 2022]. In fact, the topology of magnetic fields in *CME* can be more complex. *CME* with open field lines have been detected, and even such *CME* where both closed and open fields were present [Bothmer et al., 1996; Davies et al., 2023].

Coronal mass ejections, *CME* , are typically associated with flare activity, therefore the maximum number of such transient events occurs during solar cycle maxima [Webb et al., 2001]. Corotating solar wind streams *CIR* from coronal holes dominate on the descending branch and during solar activity minima [Valchuk et al., 1978; Simon and Legrand, 1989].

In cases where historical auroras serve as indirect data on solar activity, these must be events that have significant visible brightness and extend to middle and low latitudes. This is a necessary condition for such events in distant epochs to have been noticed by a sufficiently large number of people and recorded in historical chronicles. It is precisely these very intense auroras, visible at middle and low latitudes, that are caused by very intense magnetic storms with sudden

commencement, superstorms, the source of which are *CME* [Borovsky and Denton, 2006]. In the works [Meng et al., 2019; Cliver et al., 2022], it was found that the solar sources of very intense storms (storm index *Dst* <200 nT) are exclusively *CME* from large active regions located close to the Sun's equator. Thus, SN_1 reflects the number of precisely such active regions and is associated with local closed magnetic fields.

Data SN_2 are based on the reconstruction of CR variations obtained from ^{14}C archives in tree rings. Plasma clouds coming from the Sun fill the heliosphere and serve as a magnetic shield for galactic CRs, thereby hindering their arrival to Earth. Therefore, there is an inverse correlation with *W/SN* . For CRs, an 11-year cycle is also visible, but its maxima are somewhat shifted compared to the maxima of Wolf numbers. This is due to the significant influence of global large-scale fields on the heliosphere, the variation of which is phase-shifted relative to the Wolf number cycle [Obridko and Nagovitsyn, 2017]. In the case when indirect data on SA are based on accounting for the relationship between CR flux and ^{14}C concentration in tree rings, the integral influence on the heliosphere and magnetosphere of SA changes is taken into account, which are determined by changes in both local and global solar magnetic fields. The Sun's magnetic field demonstrates a unified organization. Local closed and large-scale open magnetic fields are interconnected, and there are reasons to believe that at different phases of the cycle they can transform into each other [Obridko and Nagovitsyn, 2017]. Therefore, in the spectra of SN_1 and SN_2 both common trends and some differences are revealed, which may be caused by greater or lesser contributions of different types of magnetic fields to the series SN_1 and SN_2 at a certain point in time.

7. CONCLUSION

In this work, a spectral analysis of sunspot number series in the range of periods greater than the Hale magnetic cycle (~22 years) and less than the Gleissberg cycle (50-120 years) on the scale of the last millennium (1000-1900) was conducted. For the study, reconstructions based on the number of low-latitude auroras SN_1 and the concentration of ^{14}C in tree rings SN_2 were used. It was found that in the spectra of SN_1 and SN_2 two stable variations with periods of ~30 and ~40 years are observed, and such cyclicity is present even during the grand minima of Oort, Wolf, Spörer, and Maunder, as well as during prolonged maxima. The source of this variation is frequency modulation by a longer-wave process, namely the approximately two-hundred-year Suess cycle (T_m=188±9 years for the series SN_1 and 205±53 years for the series SN_2) of the main oscillation with a period of T_0=35±1 years. As a result, a three-frequency structure is formed with a main period of ~35 years and side branches with periods of ~30 and ~40 years. The main frequency is poorly distinguished against the background of the side branches. However, our analysis showed that, nevertheless, the

carrier frequency significantly manifests itself in the spectrum. This makes it possible to consider that the oscillation with a period of 35 years may be a solar source of the Brückner climate cycle.

Our results suggest that in solar activity there exists a hierarchy of cycles connected by modulation effects: longer-wave cycles influence the generation of short-wave ones. Such a hierarchical system of oscillators and modulators may be responsible for creating a stable rhythmic structure in solar activity with a main period of ~35 years.

The conclusions of our study are drawn from the examination of spectra of two series of completely independent data SN_1 and SN_2, which increases confidence in the obtained results. Some difference observed in the changes of 30- and 40-year components in the spectra of series SN_1 and SN_2 in 1000-1900 may be due to differences in the methods of data reconstruction for these series. The reconstruction of SN_1 reflects variations of closed solar magnetic fields, while SN_2 reflects both closed and open fields. The Sun's magnetic field functions as a unified system that includes all types of fields, therefore the results of our analysis of SN_1 and SN_2 demonstrate the same general trends, and the difference in the obtained spectra may be related to the greater or lesser contribution of different types of magnetic fields to the series SN_1 and SN_2.

CONFLICT OF INTERESTS

The authors declare no conflict of interest.

REFERENCES

1. *Baskakov S.I.* Radio engineering circuits and signals. Moscow: Lenard, 528 p. 2016.
2. *Valchuk T.E., Livshits M.A., Feldstein Ya.I.* Probing the high-latitude magnetic field of the Sun with the geomagnetic field // Letters to Astron. J. Vol. 4. No. 11. P. 515–519. 1978.
3. *Vit insky Yu.A., Kopetsky M., Kuklin G.V.* Statistics of sunspot formation activity of the Sun. Moscow : Nauka, 296 p. 1986.
4. *Gonorovsky I.S.* Radio engineering circuits and signals. Moscow: Soviet Radio, 608 p. 1977.
5. *Landa P.S.* Nonlinear oscillations and waves. Moscow: Nauka, 495 p. 1997.
6. *Nagovitsyn Yu.A.* Solar activity of the last two millennia: "Solar Service" in ancient and medieval China // Geomagnetism and Aeronomy. Vol. 41. No. 5. P. 711–720. 2001.
7. *Nagovitsyn Yu.A.* Changes in cyclic characteristics of solar magnetic activity on long time scales // Geomagnetism and Aeronomy. Vol. 54. No. 6. P. 723–729. 2014. https://doi.org/10.7868/S0016794014060133

8. *Obridko V.N., Kanonidi Kh.D., Mitrofanova T.A., Shelting B.D.* . Solar Activity and Geomagnetic Disturbances // Geomagnetism and Aeronomy. V. 53. No. 2. P. 157-166. 2013. https://doi.org/10.7868/S0016794013010148
9. *Obridko V.N., Nagovitsyn Yu.A.* Solar Activity, Cyclicity and Forecast Methods. St. Petersburg: VVM, 466 p. 2017.
10. *Ptitsyna N.G., Tyasto M.I., Khrapov B.A.* 22-Year Cycle in the Frequency of Aurora Borealis Appearances in the 19th Century: Latitudinal Effects // Geomagnetism and Aeronomy. V. 57. No. 2. P. 208-216. 2017. https://doi.org/10.7868/S0016794017020110
11. *Ptitsyna N.G., Demina I.M.* Reconstruction of Solar Activity in 1000-1700 Based on Aurora Data Considering the Contribution of Earth's Main Magnetic Field // Geomagnetism and Aeronomy. V. 60. No. 4. P. 515-527. 2020. https://doi.org/10.31857/S0016794020030153
12. *Ptitsyna N.G., Demina I.M.* Frequency Modulation as a Cause of Additional Branches of the Gleissberg Century Cycle in Solar Activity // Geomagnetism and Aeronomy. V. 62. No. 1. P. 52-66. 2022. https://doi.org/10.31857/S0016794022010163
13. *Ptitsyna N.G., Demina I.M.* The Influence of the Gleissberg Cycle on Variations of the 11-Year Solar Activity Cycle Period in 1700-2021 // Geomagnetism and Aeronomy. V. 63. No. 3. P. 284-297. 2023. https://doi.org/10.31857/S0016794022600508
14. *Ptitsyna N.G., Demina I.M.* The Schwabe Solar Cycle in 1000-1700: Variations in Length and Amplitude // Geomagnetism and Aeronomy. V. 64. No. 2. P. 217 – 229. 2024. https://doi.org/10.31857/S0016794024020059
15. *Bertello L., Pevtsov A.A., Ulrich P.K.* 70 years of chromospheric solar activity and dynamics // Astrophys. J. V. 897. N 2. P. 181-195. 2020. https://doi.org/10.3847/1538-4357/ab9746
16. *Brehm N., Bayliss A., Christl M. et al* . Eleven-year solar cycles over the last millennium revealed by radiocarbon in tree rings // Nat. Geosci. V. 14. P. 10-15. 2021. https://doi.org/10.1038/s41561-020-00674-0
17. *Borovsky J.E., Denton M.H.* Differences between CME-driven storms and CIR-driven storms // J. Geophys. Res. V. 111. N 7. ID A07S08. 2006. https://doi.org/10.1029/2005jA011447
18. *Bothmer V., Desai M.I., Marsden R.G., Sanderson T.R., Trattner K.J., Wenzel K.-P., Gosling J.T., Balogh A., Forsyth R.J., Goldstein B.E.* ULYSSES observations of open and closed magnetic field lines within a coronal mass ejection // Astron. Astrophys . V. 316. N 2. P. 493–498. 1996.
19. *Brückner E.* Climate fluctuations since 1700. Vienna, Olmütz: Ed. Hölzel, 325 p. 1890.

20. *Cliver E.W., Pötzi W., Veronig A.M.* Large sunspot groups and great magnetic storms: Magnetic suppression of CMEs // Astrophys. J. V. 938 . N 2 . ID 136. 2022. https://doi.org/10.3847/1538-4357/ac847d
21. *Clilverd M.A., Clarke E., Ulich T., Rishbeth H., Martin J.* Predicting solar cycle 24 and beyond // Space Weather. V. 4. N 9. ID S09005. 2006. https://doi.org/10.1029/2005SW000207
22. *Connor F.R.* Modulation. London: Edward Arnold Ltd., 133 p. 1982.
23. *Daubechies I.* Ten lectures on wavelets. Philadelphia, PA: Society for industrial and applied mathematics, 369 p. 1992. https://doi.org/10.1137/1.9781611970104
24. *Davies E.E, Scolini C., Winslow R.M., Jordan A.P., Möstl C.* The effect of magnetic field line topology on ICME-related GCR Modulation // Astrophys. J. V. 959 . N 2 . ID 133. 2023. https://doi.org/10.3847/1538-4357/ad046a
25. *Echer E., Rigozo N.R., Nordemann D.J.R., Vieira L.E.A.* Prediction of solar activity on the basis of spectral characteristics of sunspot number // Ann. Geophys. V. 22. N 6. P. 2239–2243. 2004. https://doi.org/10.5194/angeo-22-2239-2004
26. *Eddy J.A.* The historical record of solar activity / The ancient sun: Fossil record in the earth, moon and meteorites / Proceedings of the Conference. Boulder. CO. October 16–19, 1979. (A81-48801 24-91). New York, Oxford: Pergamon Press. P. 119–134. 1980.
27. *Gonzalez W.D., Joselyn J.A., Kamide Y., Kroehl H.W., Rostoker G., Tsurutani B.T., Vasyliunas V.M* . What is a geomagnetic storms? // J. Geophys. Res. V. 99. N 4. P. 5771-5792. 1994 . https://doi.org/10.1029/93JA02867
28. *Grossmann A., Morlet J.* Decomposition of Hardy functions of constant shape // SIAM J. Math. Anal. V. 15. N 4. P.723-736. 1984. https://doi.org/ 10.1137/0515056
29. *Gopalswamy N.* The sun and space weather // Atmosphere. V. 13. N 11. ID 1781. 2022. https://doi.org/10.3390/atmos13111781
30. *Feynman J.,* Gabriel S.B. Period and phase of the 88-year solar cycle and the Maunder minimum: Evidence for a chaotic sun // Sol. Phys. V. 127. N 2. P. 393-403. 1990. https://doi.org/10.1007/BF00152176
31. *Feynman J., Ruzmaikin A.* The Centennial Gleissberg Cycle and its association with extended minima // J. Geophys. Res. - Space. V. 119. N 8. P. 6027-6041. 2014. https://doi.org/10.1002/2013JA019478

32. *Kane R. P.* Prediction of the sunspot maximum of solar cycle 23 by extrapolation of spectral components // Sol. Phys. V. 189. N 1. P. 217-224. 1999. https://doi.org/10.1023/A:1005298313886
33. *Keimatsu M., Fukushima N., Nagata T.* Archaeo-aurora and geomagnetic secular variation in historic time // J. Geomagn. Geoelectr. V. 20. N 1. P. 45-50. 1968. https://doi.org/10.5636/jgg.20.45
34. *Kudsk S.G., Knudsen M.F., Karoff C., Baittinger C., Misios S., Olsen J.* Solar variability between 650 CE and 1900 - Novel insights from a global compilation of new and existing high-resolution ^{14}C records // Quaternary Sci. Rev. V. 292. ID 107617. 2022. https://doi.org/10.1016/j.quascirev.2022.107617
35. *Liritzis Y., Petropoulos B.* Latitude dependence of auroral frequency in relation to solar-terrestrial and interplanetary parameters // Earth Moon Planets. V. 39. N 1. P. 75-91. 1987. https://doi.org/10.1007/BF00054435
36. *McCracken K.G., Beer J., Steinhilber F., Abreu J.* A phenomenological study of the cosmic ray variations over the past 9400 years, and their implications regarding solar activity and the solar dynamo // Sol. Phys. V. 286. N 2. P. 609−627. 2013. https://doi.org/10.1007/s11207-013-0265-0
37. - *Meng X., Tsurutani B.T. , Mannucci A.J.* The solar and interplanetary causes of superstorms (minimum *Dst* ≤ −250 nT) during the space age // J. Geophys. Res. V. 124. N 6 . P. 3926-3948. 2019. https://doi.org/10.1029/2018JA026425
38. *Muscheler R., Joos F., Beer J., Müller S.A., Vonmoos M., Snowball I.* Solar activity during the last 1000 yr inferred from radionuclide records // Quaternary Sci. Rev. 2006. V. 26. N 1-2 . P. 82-97. 2006. https://doi.org/10.1016/j.quascirev.2006.07.012
39. *Peristykh A.N., Damon P.E* . Persistence of the Gleissberg 88 year cycle over the last ~12,000 years: Evidence from cosmogenic isotope // J. Geophys. Res. − Space. V. 108. N 1. ID 1003. 2003. https://doi.org/10.1029/2002JA009390
40. *Petrovay K.* Solar cycle prediction // Living Rev. Sol. Phys. V. 17. ID 2. 2020. https://doi.org/10.1007/s41116-020-0022-z
41. *Raspopov O.M., Shumilov O.I, Kasatkina EA, Turunen E., Lindtholm M.* 35-year climatic Bruckner cycle - solar control of climate variability? / Proc. 1 st Solar and Space weather Euroconference "The solar cycle and terrestrial climate". Santa Cruz de Tenerife, Spain. September 25-29, 2000. Ed. A. Wilson. Noordwijk, Netherlands: ESA Publications Division. P. 517. 2000.

42. *Schove D.J.* Aurora numbers since 500 B.C. // Journal of the British Astronomical Association. V.72. N 1. P. 31-35. 1962.
43. *Silverman S.M* . Secular variation of the aurora for the past 500 years // Rev. Geophys. V. 30. N 4. P. 333-351. 1992. https://doi.org/10.1029/92RG01571
44. *Simon P.A., Legrand J.P* . Solar cycle and geomagnetic activity: A review for geophysicists. Part II. The solar sources of geomagnetic activity and their links with sunspot cycle activity // Ann. Geophys. V. 7. N 6. P. 579-593. 1989.
45. *Siscoe G.L.* Evidence in the auroral record for secular solar variability // Rev. Geophys. V. 18. N 3. P. 647-658. 1980. https://doi.org/10.1029/RG018i003p00647
46. *Singh Y.P., Badruddin B.* Prominent short-, mid-, and long-term periodicities in solar and geomagnetic activity: Wavelet analysis // Planet. Space Sci. V. 96 . P. 120-124. 2014. https://doi.org/10.1016/j.pss.2014.03.019
47. *Svalgaard L.* Up to nine *millennia* of multimessenger solar activity // arXiv Preprint: 1810.11952. 2018. https://arxiv.org/ftp/arxiv/papers/1810/1810.11952.pdf
48. *Travers R., Usoskin I.G., Solanki S.K., Becagli S., Frezzetti M., Severi M., Stenni B., Udisti R* . Nitrate in polar ice: a new tracer of solar variability // Sol. Phys. V. 280. N 1. P. 237-254. 2012. https://doi.org/10.1007/s11207-012-0060-3
49. *Tsurutani B., Gonzalez W., Gonzalez A.L.C. et al.* Corotating solar wind streams and recurrent geomagnetic activity: a review // J. Geophys. Res. V. 111. N 7. ID A07S01. 2006. https://doi.org/10.1029/2005JA011273
50. *Usoskin I.G.* A history of solar activity over millennia // Living Rev. Sol. Phys. V. 14. ID 3. 2017. https://doi.org/10.1007/s41116-017-0006-9
51. *Usoskin I.G., Solanki S.K., Kovaltsov G.A.* Grand minima and maxima of solar activity: new observational constraints // Astron. Astrophys. V. 471. N 1. P. 301-309. 2007. https://doi.org/10.1051/0004-6361:20077704
52. *Usoskin I.G., Solanki S.K., Krivova N., Hofer B., Kovaltsov G.A., Wacker L., Brehm N., Kromer B.* Solar cycle activity over the last millennium reconstructed from annual 14C data // Astron. Astrophys. V. 649. ID A141. 2021. https://doi.org/10.1051/0004-6361/202140711
53. *Vazquez M., Vaquero J.M., Gallego M.C* . Long-term spatial and temporal variations of aurora borealis events in the period 1700-1905 // Sol. Phys. V. 289. N 5. P. 1843-1861. 2014. https://doi.org/10.1007/s11207-013-0413-6

54. *Veretenenko S., Ogurtsov M., Obridko V* . Long-term variability in occurrence frequencies of magnetic storms with sudden and gradual commencements // J. Atmos. Sol. - Terr. Phy. V. 205. ID 105295. 2020. https://doi.org/10.1016/j.jastp.2020.105295

55. *Webb D.F., Crooker N.U., Plunkett S.P., St. Cyr O.C.* The solar sources of geoeffective structures / Space Weather: Progress and Challenges in Research and Applications. Eds. P. Song, H.J. Singer, G. Siscoe / Geophysical Monograph Series. V. 125. Washington, DC: AGU. P. 123-141. 2001. https://doi.org/10.1029/GM125p0123

FIGURE CAPTIONS

Fig. 1. Reconstructed series of solar activity. (*a*) – series SN_1 based on auroras, (*b*) – series ^{14}C SN_2; (*c*) – smoothed and normalized series: solid line shows series SN_1, dashed line – series SV_2 **.** Grand minima are marked with vertical lines.

Fig. 2. Spectra of the analyzed time series before (*a*) and after filtration (*b*).

Fig. 3. Wavelet spectrum of the time series SN_1. Contour lines represent the modulus of wavelet coefficients, circles indicate maxima of the 30-year component, diamonds indicate maxima of the 40-year component.

Fig. 4. Change in the period of 30-40-year components found from the wavelet spectrum of SN_1 and predicted within the hypothesis of long-wave signal modulation. Circles denote periods of the 30-year component, diamonds – the 40-year component, filled symbols – obtained from the wavelet spectrum, unfilled symbols – predicted.

Fig. 5. Wavelet spectrum of the time series SN_2. The symbols are the same as in Fig. 3, the main oscillation period with a period of T =35±1 years is marked with asterisks.

Fig. 6. Change in the period of 30- and 40-year components found from the wavelet spectrum spectrumSN_2 and predicted within the framework of the hypothesis of modulation by a long-wave signal. The symbols are the same as in Fig. 4.

Fig. 7. Comparison of the predicted branches of the 35-year main oscillation from wavelet spectra spectraSN_1 and SN_2. Symbols ○ denote the predicted periods of the 30-year branch of SN_2, symbols ◇ – the same for the 40-year branch, ✲ – the same for the 30-year and ✳ – 40-year branch of SN_1.

Fig. 8. Cross-correlation functions of the 40-year (*a*) and 30-year (*b*) spectral components in SN_1 and SN_2. Arrows mark the maxima discussed in the text.

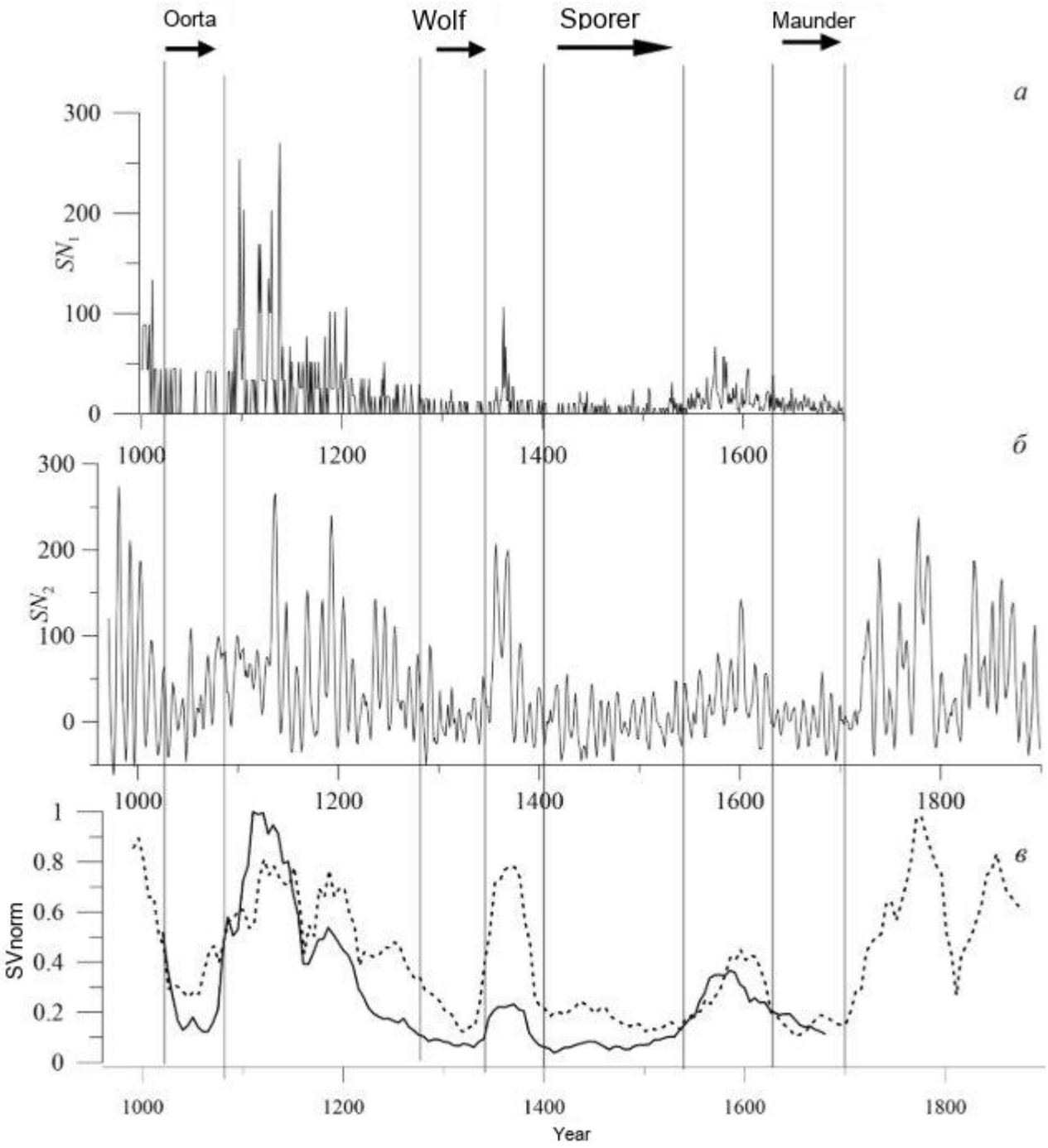

Fig. 1.

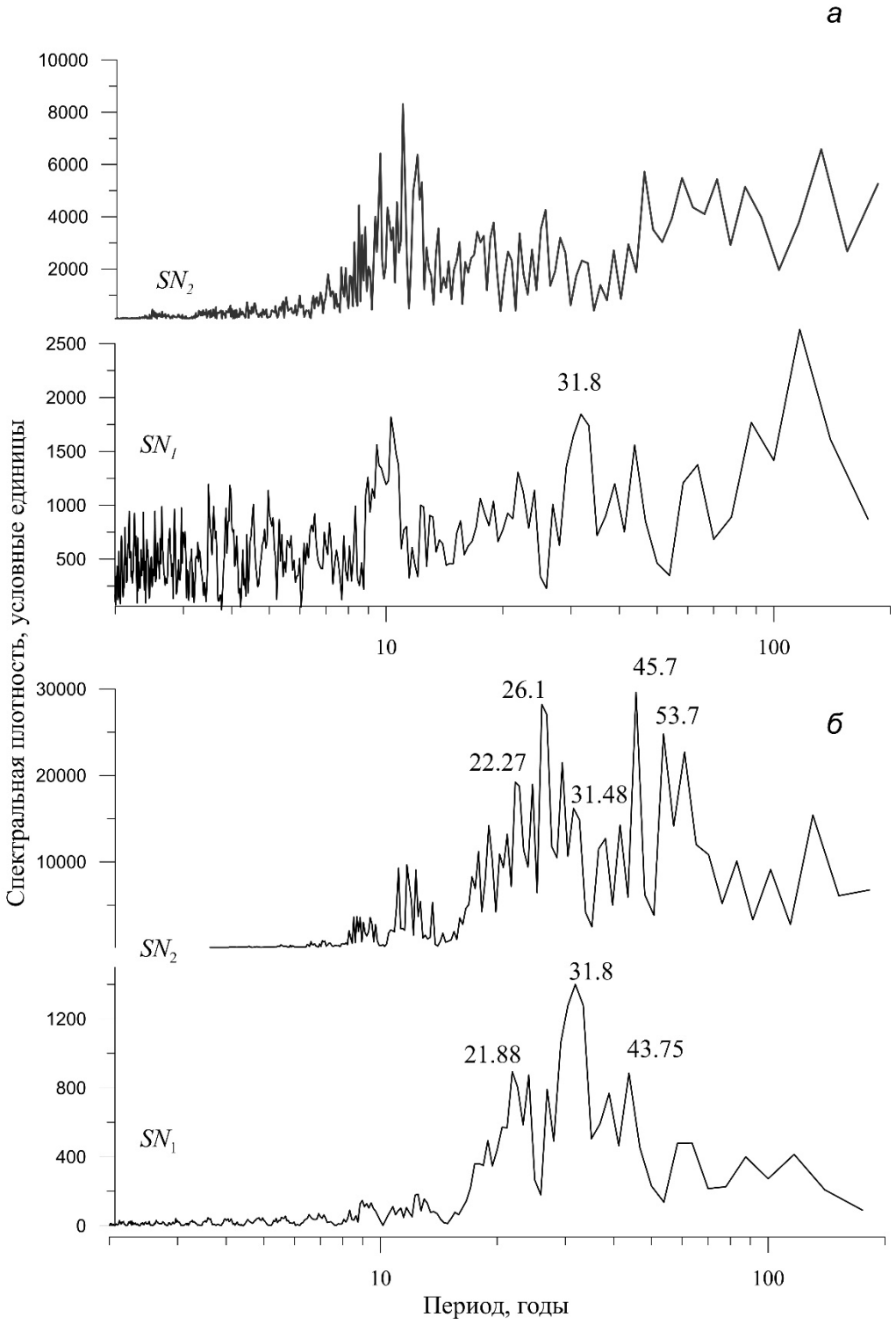
а
10000
8000
6000
4000
2000
SN_2
2500
2000
1500
1000
500
SN_1
31.8
10
100
Спектральная плотность, условные единицы
30000
20000
10000
SN_2
26.1
45.7
53.7
22.27
31.48
б
1200
800
400
0
SN_1
31.8
21.88
43.75
10
100
Период, годы

Fig. 2.

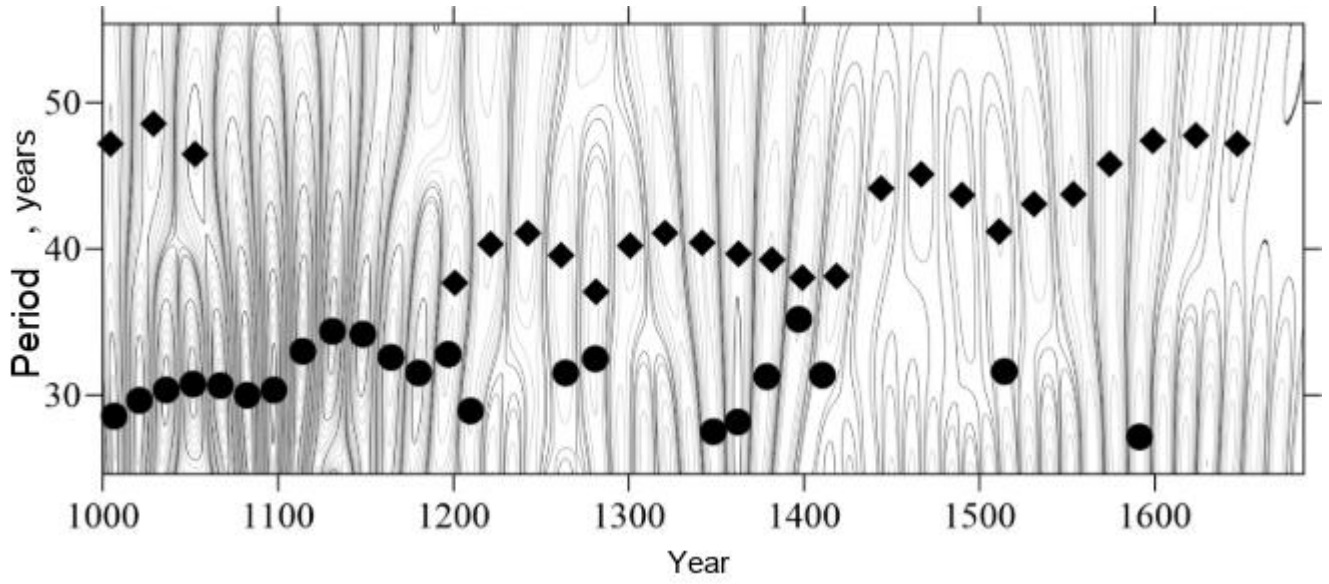
Period , years
50
40
30
1000
1100
1200
1300
1400
1500
1600
Year

Fig. 3.

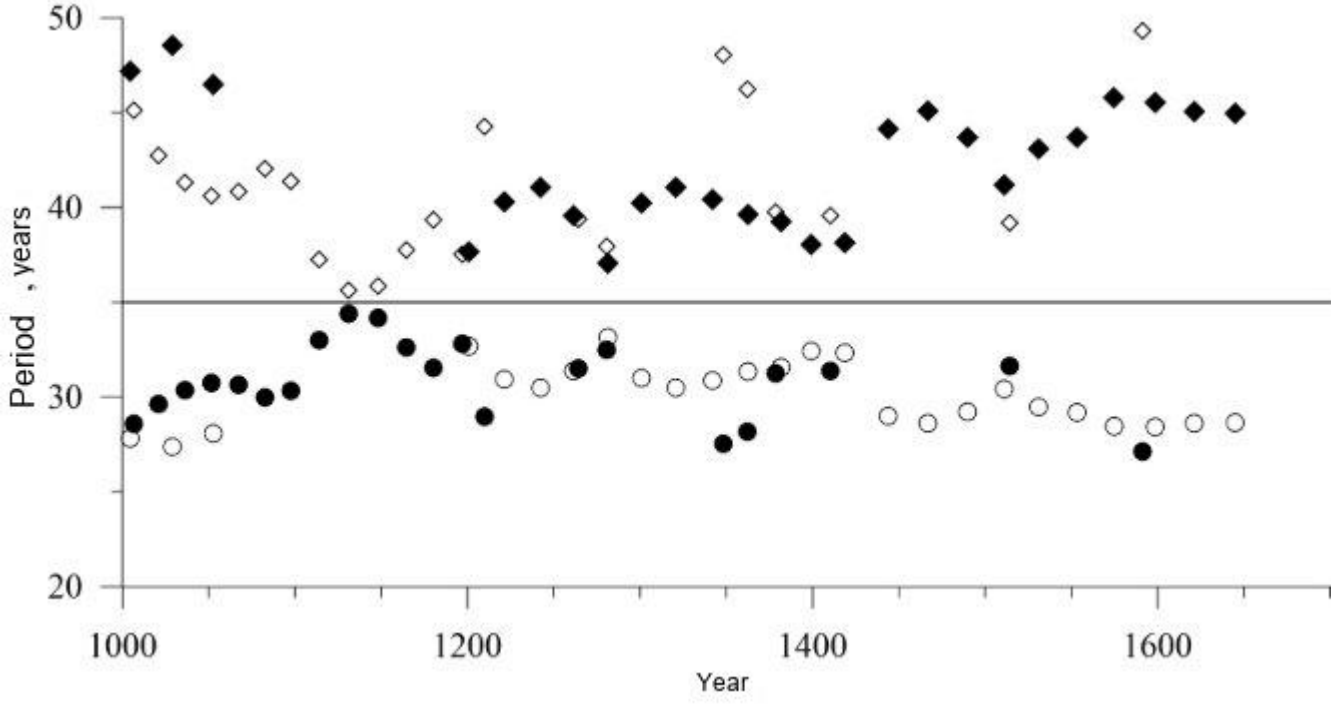
Period , years
50
40
30
20
1000
1200
1400
1600
Year

Fig. 4.

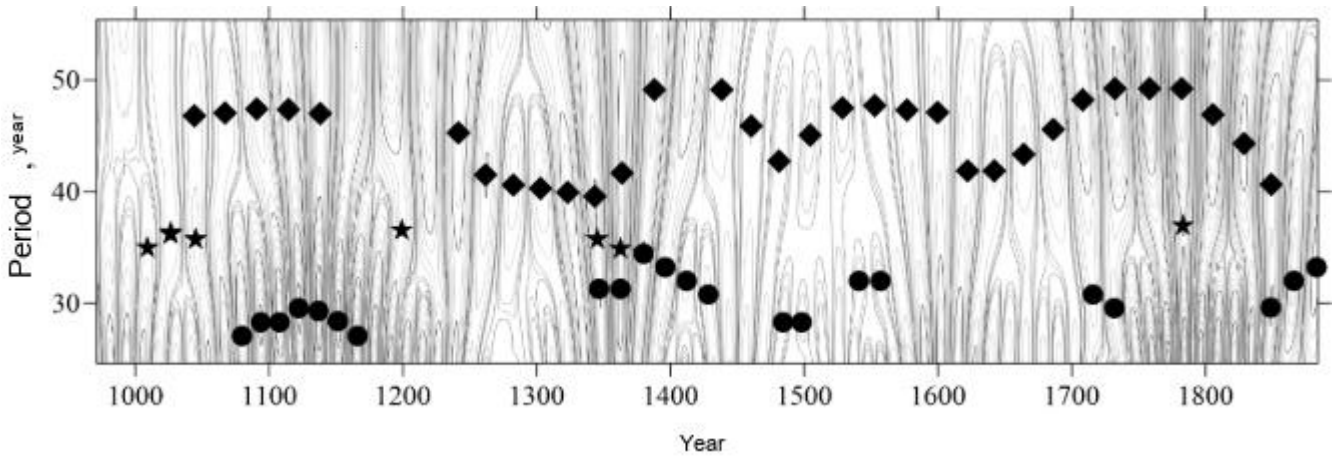
Period , year
50
40
30
1000
1100
1200
1300
1400
1500
1600
1700
1800
Year

Fig. 5.

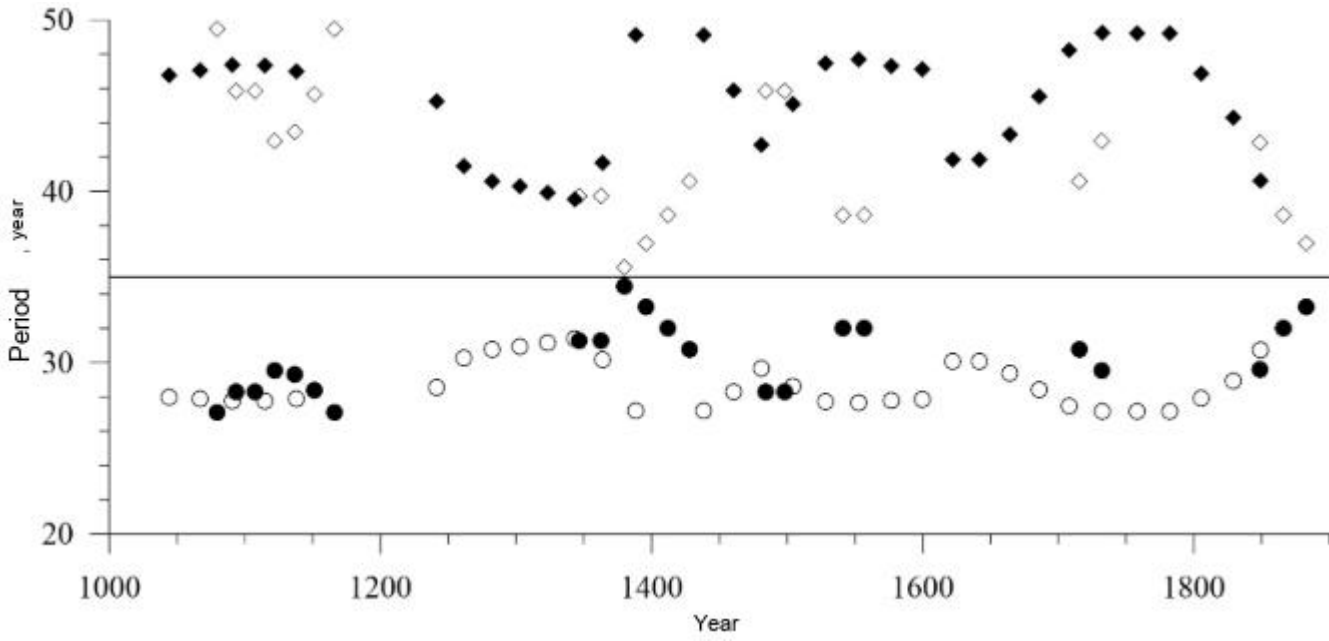
Period , year
50
40
30
20
1000
1200
1400
1600
1800
Year

Fig. 6.

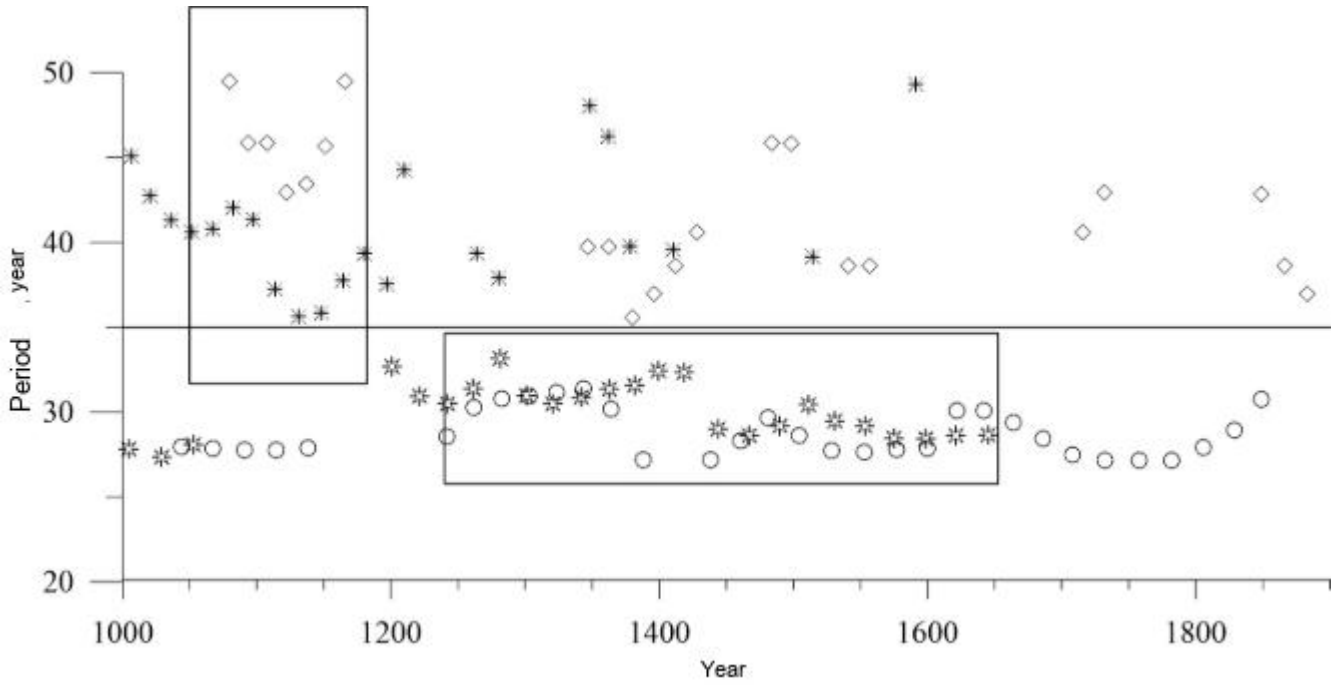

Fig. 7.

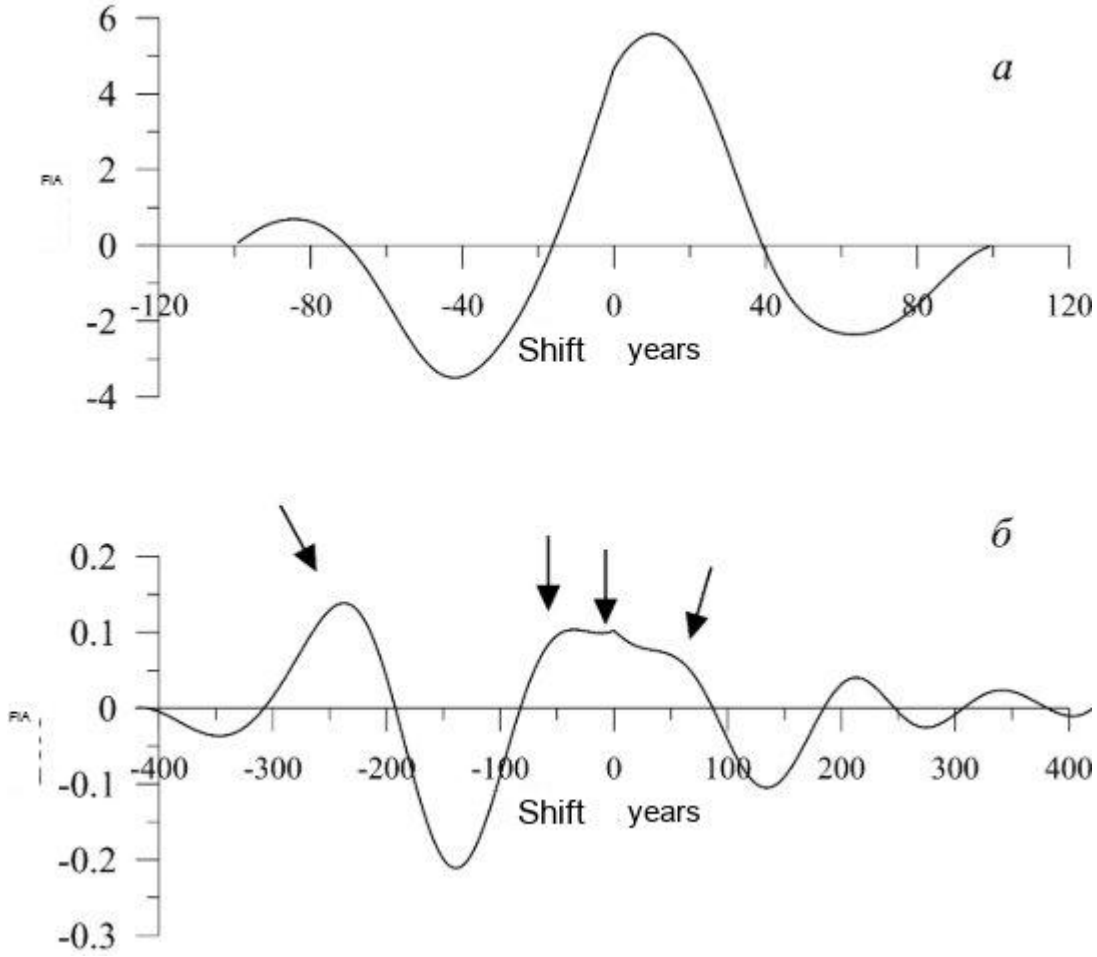
а
6
4
2
0
-2
-4
-120
-80
-40
0
40
80
120
Shift years
б
0.2
0.1
0
-0.1
-0.2
-0.3
-400
-300
-200
-100
0
100
200
300
400
Shift years

Fig. 8.